SIAM J. APPL. MATH.
Vol. 70, No. 7, pp. 2750–2770

VARIATIONAL FUZZY MUMFORD–SHAH MODEL FOR IMAGE SEGMENTATION*

FANG LI†, MICHAEL K. NG‡, AND CHUNMING LI§

Abstract. In this paper, we propose a variational fuzzy Mumford–Shah model for image segmentation. The model is based on the assumption that an image can be approximated by the product of a smooth function and a piecewise constant function. Image segmentation is achieved by minimizing the energy functional in terms of membership functions, which take values between 0 and 1 to accommodate the uncertainty of the membership of the pixels, and the partial volume effect in medical images. We show the existence and symmetry of minimizers for the proposed energy minimization problem. The energy can be minimized by an efficient iterative algorithm. Our iterative method has been applied to medical images and natural images with good results. Comparisons with other segmentation methods demonstrate the advantage of our method in the presence of intensity inhomogeneities.

Key words. Mumford–Shah model, segmentation, total variation, fuzzy membership functions, operator splitting

AMS subject classifications. 65K10, 68U10, 90-08

DOI. 10.1137/090753887

1. Introduction and motivation.

Image segmentation is a fundamental task in image processing and computer vision. It is aimed to partition an image into a number of regions corresponding to the objects in the image. Variational methods have been increasingly used as powerful methods for image segmentation. In variational formulation, image segmentation is achieved by solving an energy minimization problem, which allows conveniently integrating a variety of useful information, such as shape prior, and constraints on the regularity of object boundaries.

Many variational models for image segmentation have been proposed in the past two decades. Well-known variational models for image segmentation include Mumford–Shah model [24], region competition [36], geodesic active contour [7], geodesic active region [28]. The energy functionals in most of the existing variational models are not convex in the optimization space. Consequently, many variational models are plagued with local minima problems. As a result, these methods are sensitive to initialization.

To overcome the above mentioned drawback, recently Chan, Esedoglu, and Nikolova [26] and Bresson et al. [5] proposed new variational frameworks in which fuzzy membership functions are introduced to represent the regions such that the new functionals are convex with respect to the membership function. Global minimum can be achieved in these models due to the convexity of the energy functional. Obviously,

*Received by the editors March 25, 2009; accepted for publication (in revised form) June 17, 2010; published electronically August 19, 2010.
http://www.siam.org/journals/siap/70-7/75388.html
†Department of Mathematics, East China Normal University, Shanghai, China (lifangswnu@126.com). This author's research was supported in part by the Doctoral Program of Higher Education (200802691037) and the National Science Foundation of Shanghai (10ZR1410200).
‡Corresponding author. Centre for Mathematical Imaging and Vision and Department of Mathematics, Hong Kong Baptist University, Kowloon Tong, Hong Kong (mng@math.hkbu.edu.hk). This author's research was supported in part by HKRGC grants and HKBU FRGs.
§Institute of Imaging Science, Vanderbilt University, Nashville, TN 37232 (chunming.li@vanderbilt.edu).

these models are not sensitive to initialization. Another advantage of the method in [5] is the use of the auxiliary variable to approximate the membership function, which allows a closed form solution of the membership function and the use of Chambolle's fast dual projection method [8] to solve the auxiliary variable. This technique has been widely used in many other models [22, 23, 6, 25]. However, this technique is used only in two-phase segmentation, and it is not trivial to be extended to multiphase models. A general multiphase stochastic variational fuzzy segmentation model was proposed by Shen [31] based on the Mumford–Shah model. The author used stochastic variables to represent the ownership of each class, which are regularized by a regularization term with a double well potential. However, the energy functional in this model is nonconvex. Moreover, a set of PDEs with respect to the stochastic variables have to be solved, which makes the implementation computationally expensive.

Intensity inhomogeneity (i.e., bias field) occurs in many real world images from different modalities, such as x-ray radiography/tomography and magnetic resonance (MR) images. In particular, the intensity inhomogeneity in MR images arises from the nonuniform magnetic field produced by radiofrequency coils as well as from object susceptibility. This phenomenon also occurs in natural images which is usually caused by nonuniform illumination. Intensity inhomogeneity causes serious errors when using piecewise constant models, such as the Chan–Vese model [9]. In fact, intensity inhomogeneities can be handled by more complicated region-based models, such as the Mumford–Shah model. However, the Mumford–Shah model is difficult to implement since it uses regions/curve as variables. Moreover, the Mumford–Shah model is computationally very expensive, which limits its practical application. Vese and Chan [33] proposed to use the level set to represent the regions/curve and reformulated the Mumford–Shah model; thereby, the problem can be solved in a level set framework [27]. However, the computation is still expensive, as a set of PDEs have to be solved during the level set evolution to obtain the smooth functions that approximate the image in the regions to be segmented. Simultaneously, Tsai, Yezzi, and Willsky [32] proposed essentially the same method as [33] to implement the Mumford–Shah functional. Recently, advances have been made to reduce computational costs of this approach such as Newton-type iterations [16] and Lagrangian representations [10]. Li et al. [18] proposed a more efficient level set–based algorithm by using the kernel function to integrate the neighborhood influence. Their method is, however, sensitive to initialization when a small scale parameter of the kernel function is used. Topological derivative is another technique used to reduce iterations needed to reach a minimum when solving the piecewise constant/smooth Mumford–Shah model; see [14, 15].

To deal with intensity inhomogeneities, several methods for segmentation have been proposed in conjunction with bias correction. Expectation-maximization (EM) and fuzzy c-means (FCM) techniques have been widely employed in these methods [34]. Wells et al. in [35] proposed an EM algorithm to solve the bias correction problem and the tissue classification problem. The disadvantage of this EM method is that it is sensitive to initialization. The FCM clustering method [4] is widely used in data classification. However, the FCM is sensitive to noise and it cannot handle the intensity inhomogeneity. Pham and Prince [29] proposed an adaptive fuzzy c-means (AFCM) method, in which the constant cluster centers are replaced by spatially varying functions with the bias field as multiplicative components. Smoothness of the bias field is ensured by penalizing its first and second order derivatives, which leads to a computationally expensive procedure for the smoothing of the bias field. Additionally, it is sometimes difficult to choose an appropriate weight for the regularization term. Li et al. [19] derived a combined model based on the maximum a posteriori

probability principle. The energy is similar to the AFCM model but adding a new neighborhood term which ensures the regularization on membership functions. The method outperforms the AFCM algorithm. However, the computation of bias field is also expensive. Ahmed et al. [1] proposed to add a neighborhood term that enabled the class membership of a pixel to be influenced by its neighbors. The neighborhood effect acts as a regularizer and forces the solution toward a piecewise homogeneous labeling. This approach proved tolerance to salt and pepper noise, resulting in smoother segmentation. Li et al. [17] proposed a variational level set–based method for medical image segmentation and bias correction. In view of an observation that local intensities form separable clusters, they define a clustering objective function for local intensities, which is then integrated to define an energy functional in terms of level set functions and a bias field. Since the smoothness of the bias field is intrinsically implied in the clustering objective function, no extra effort is needed to smooth the computed bias field. However, the level set formulation is not convenient for representing an arbitrary number of regions, and the numerical scheme for the level set evolution is computationally expensive.

In this paper, we propose a new multiphase fuzzy Mumford–Shah segmentation model for images with intensity inhomogeneity. Our basic assumption is that a piecewise smooth image can be approximated by the product of a piecewise constant function and a smooth function. The smooth function is used to estimate the bias field in the image. Based on this assumption, we combine the original Mumford–Shah model with the FCM method by using fuzzy membership functions to represent regions. The proposed functional is convex with respect to each fuzzy membership function. We will show the existence and symmetry of minimizers for the proposed energy minimization problem. We provide an iterative algorithm to solve the energy minimization problem which is fast and easy to implement. In the algorithm, the piecewise constant function is given by the closed form solution and the bias field is solved by the Gauss–Seidel iteration method. Minimizing the membership functions are not direct since there are total variation terms in the energy and two constraints on the membership functions. We propose to use the operator splitting method in the Euler–Lagrange equations of membership functions by introducing new variables in these equations such that all the involved variables have closed form solutions. Experimental results show that the quality of image segmentation results by using the fuzzy Mumford–Shah model is desirable.

We remark that in [15] the authors also consider a functional with a product of a smooth function and a piecewise constant function and then derived an energy (i.e., (3.3) in this paper) from the Mumford–Shah functional. Different from [15] in which the authors solve the hard segmentation problem (3.3) with topological derivative and level set method, in this paper, we solve the problem in a new fuzzy framework and design novel numerical algorithm.

This paper is outlined as follows. In section 2, we review some previous work. In section 3, we present and study the new model. In section 4, we develop the numerical algorithm. In section 5, we show the experimental results. Then we conclude the paper in section 6.

2. Previous work. The general N-phase segmentation problem can be formulated as follows: Given an image $I : \Omega \to \mathbb{R}$ where the image domain Ω is a rectangle in $\mathbb{R}^2$, the aim is to partition Ω into N disjoint connected open subsets $\{\Omega_i\}_{i=1}^N$ by certain suitable measures such that $\Omega_1 \cup \cdots \cup \Omega_N \cup \Gamma = \Omega$, where Γ is the union of the part of boundaries of the Ω_i inside Ω.

2.1. The Mumford–Shah model. In 1989, Mumford and Shah [24] proposed to solve this segmentation problem by minimizing the following energy:

$$E_{\mathrm{MS}}(g,\Gamma) = \lambda \int_{\Omega} (I-g)^2 dx + \mu \int_{\Omega-\Gamma} |\nabla g|^2 dx + |\Gamma|, \tag{2.1}$$

where $|\Gamma|$ stands for the total length of the arcs making up Γ, and λ, μ are the weight parameters. The interpretation of the three terms is as follows: The first term requires that g approximates I; the second term requires that g does not vary very much on each Ω_i; the third term requires that the boundary Γ be as short as possible. Here g is a piecewise smooth approximate function of image I. In particular, Mumford and Shah considered the special case where the function g is chosen to be a piecewise constant function.

2.2. The fuzzy *c*-means method. The standard FCM objective function for partitioning image I into N regions (the continuous form of FCM energy in [4]) is given by

$$E_{\mathrm{FCM}}(U,c) = \sum_{i=1}^{N} \int_{\Omega} (I(x)-c_i)^2 u_i^p(x) dx, \tag{2.2}$$

where the constant c_i is the region center of class i, the function u_i is called the fuzzy membership function, $u_i(x)$ denotes the membership value (probability) for point $x \in \Omega$ to be in class i which satisfies

$$0 \le u_i \le 1 \quad \text{and} \quad \sum_{i=1}^{N} u_i = 1,$$

U denotes $(u_1, \ldots, u_N)$, and c denotes $(c_1, \ldots, c_N)$. The parameter p is a weighting exponent on each fuzzy membership function and determines the amount of fuzziness of the resulting classification.

3. The fuzzy segmentation model.

3.1. Bounded variation (BV) space and total variation. The bounded variation space $\mathrm{BV}(\Omega)$ [11] is a subspace of functions $f \in L^1(\Omega)$ such that the following quantity is finite:

$$\int_{\Omega} |\nabla f| dx := \sup \left\{ \int_{\Omega} f \mathrm{div} \varphi dx \mid \varphi \in C_c^1(\Omega, \mathbb{R}^2), |\varphi| \le 1 \right\}.$$

$\mathrm{BV}(\Omega)$ endowed with the norm

$$\|u\|_{\mathrm{BV}} = \int_{\Omega} |\nabla u| dx + \|u\|_{L^1(\Omega)}$$

is a Banach space. The term $\int |\nabla f| dx$ is called total variation of f. Here ∇f is understood as a radon measure. If $f = 1_{\mathcal{V}}(x)$ is a characteristic function of a set $\mathcal{V} \subset \Omega$, then the total variation $\int_{\Omega} |\nabla f| dx = |\partial \mathcal{V}|$, where $|\partial \mathcal{V}|$ represents the perimeter of the boundary of $\mathcal{V}$.

The BV space allows functions with discontinuities. Piecewise constant/smooth images are usually assumed to be in BV space, and total variation regularization is popular in variational image modeling [2]. On the other hand, the BV space has

the following useful compactness property: If $\{u_n\}$ is a uniformly bounded sequence in $\mathrm{BV}(\Omega)$, then up to a subsequence, also denoted as $\{u_n\}$, there exists a function $u^* \in \mathrm{BV}(\Omega)$ such that $u_n \to u^*$ in $L^1(\Omega)$ strong and $\nabla u_n \rightharpoonup \nabla u^*$ in the sense of measure. See [11] for a detailed proof.

3.2. Piecewise smooth images. In this paper, we suppose the piecewise smooth function g can be approximated by a smooth function b multiplying a piecewise constant function $\sum_{i=1}^{N} c_i \chi_i$ where χ_i is the characteristic function of set Ω_i and c_i is a constant. We also assume that an observed image is contaminated by an additive Gaussian noise. Therefore, we consider the following image model:

$$I(x) = b(x)c_i + n(x), \qquad x \in \Omega_i, \tag{3.1}$$

where $\{\Omega_i\}_{i=1}^{N}$ is a partition of the image domain Ω as described in the above. This model has been widely used in modeling images with intensity inhomogeneity [35, 29, 17]. Our goal is to recover b, $c = (c_1, \ldots, c_n)$ and the partition from the observed image I. The smooth function b models the bias field in MR images. The bias field is generally assumed to be slowly varying and to take values around 1.

We note that in the image model (3.1), if $(b, \{c_i\})$ is a solution, then after a rescaling $(kb, \{c_i/k\})$ is also a solution where k is a scaling factor. This shows that it is not possible to have the uniqueness of solution. To overcome this drawback, we assign the scale of c_i by using the following formula:

$$c_i = \frac{\int_{\Omega_i} I(x)dx}{\int_{\Omega_i} dx},$$

which computes the mean value of image I in Ω_i. In the next subsection, membership functions will be incorporated in the formula of c_i.

3.3. The fuzzy Mumford–Shah energy. In the Mumford–Shah model, we assume the piecewise smooth function $g = g_i$ on Ω_i where g_i is a smooth function defined on Ω_i. Thus, the Mumford–Shah model (2.1) can be rewritten as

$$E_{\mathrm{MS}}(g_i, \Gamma) = \sum_{i=1}^{N} \lambda \int_{\Omega_i} (I - g_i)^2 dx + \sum_{i=1}^{N} \mu \int_{\Omega_i} |\nabla g_i|^2 dx + |\Gamma|. \tag{3.2}$$

By using the image model in (3.1), the above Mumford–Shah energy can be revised as follows:

$$\hat{E}(\Gamma, b, c) = \sum_{i=1}^{N} \lambda \int_{\Omega_i} (I - bc_i)^2 dx + \mu \int_{\Omega} |\nabla b|^2 dx + |\Gamma|. \tag{3.3}$$

The second term asks that b varies smoothly. Meanwhile, to constrain that b varies in a range near one, we add another fitting term. Then the general model is to minimize

$$\hat{E}(\Gamma, b, c) = \sum_{i=1}^{N} \lambda \left(\int_{\Omega_i} (I - bc_i)^2 dx + w \int_{\Omega_i} (I - c_i)^2 dx \right) + \mu \int_{\Omega} |\nabla b|^2 dx + |\Gamma|, \tag{3.4}$$

where λ, w, μ, μ' are weighting parameters. In terms of characteristic functions $\chi = (\chi_1, \ldots, \chi_N)$, where χ is the characteristic function of Ω_i, the energy in (3.4) can be

rewritten as

$$\hat{E}(\chi, b, c) = \sum_{i=1}^{N} \lambda \int_{\Omega} \left((I - bc_i)^2 + w(I - c_i)^2 \right) \chi_i dx + \mu \int_{\Omega} |\nabla b|^2 dx + \sum_{i=1}^{N} \int_{\Omega} |\nabla \chi_i| dx, \tag{3.5}$$

where in the last term $\int_{\Omega} |\nabla \chi_i| dx$ equals the perimeter of Ω_i.

The characteristic functions χ are binary which can be used to represent a hard segmentation result. The functional $\hat{E}$ is not convex with respect to χ, and it is hard to solve numerically. However, fuzzy segmentation is preferable to hard segmentation in many applications, such as segmentation of MR images with partial volume effect. To enable fuzzy segmentation, we replace the binary characteristic functions χ_i by fuzzy membership functions u_i with the following two constraints:

$$0 \le u_i \le 1, \tag{3.6}$$

$$\sum_{i=1}^{N} u_i = 1. \tag{3.7}$$

Thus, image segmentation and bias field estimation is formulated as a problem of minimizing the following energy:

$$E(U, b, c) = \sum_{i=1}^{N} \lambda \int_{\Omega} \left((I - bc_i)^2 + w(I - c_i)^2 \right) u_i^p dx + \mu \int_{\Omega} |\nabla b|^2 dx + \sum_{i=1}^{N} \int_{\Omega} |\nabla u_i| dx, \tag{3.8}$$

where p is a parameter to determine the fuzziness of segmentation ($p > 1$). Here we set c_i as a function of fuzzy membership given by

$$\begin{cases} c_i = \dfrac{\displaystyle\int_{\Omega} I(x) u_i^p(x) dx}{\displaystyle\int_{\Omega} u_i^p(x) dx}, & \text{if } \displaystyle\int_{\Omega} u_i^p(x) dx > 0; \\ c_i = 0, & \text{if} \displaystyle\int_{\Omega} u_i^p(x) dx = 0, \end{cases} \tag{3.9}$$

and $U = (u_1, \ldots, u_N)$, $c = (c_1, \ldots, c_N)$. We note that the formula of c_i in (3.9) has been commonly used in fuzzy clustering; see, for instance, [3]. In the alternative minimization scheme discussed in the next section, we fix c and b, and then update the new value of U. Since c is defined as in (3.9) and it is related to U, the variable c in (3.8) is regarded as an intermediate variable, and it is calculated based on the current value of U.

Under the assumption the image $I \in L^{\infty}(\Omega)$, the energy (3.8) is well defined and finite for the admissible set

$$\text{adm}_N = \{U, b, c \mid u_i \in BV(\Omega), i = 1 : N, \text{satisfies (3.6) and (3.7)}, b \in H^1(\Omega), c \in \mathbb{R}^N\}.$$

Next we will prove the existence of minimizer of energy E and its symmetry property.

THEOREM 3.1. *Assume the image $I \in L^{\infty}(\Omega)$ and $I \ge 0$. Then for fixed parameters N, λ, w, and μ, there exists a minimizer of the energy E in the admissible set adm_N.*

To prove this theorem, we will use the following lemma which is an extension of the results in [31].

LEMMA 3.2. *Let $\{b_n\}$ be a sequence of functions in $L^2(\Omega)$, and $\{u_n\}$ be a sequence of nonnegative measurable functions on Ω and valued in $[0, 1]$. Suppose that*

(i) $u_n \to u_*$, *a.e. on* Ω *and* $\int_\Omega u_* dx > 0$;
(ii) $\int_\Omega b_n^2 u_n^p dx \le M_1$ *for some* $M_1 > 0$, $n = 1, \dots, \infty$.
Then there exists some function $\rho \in L^2(\Omega)$ *such that*
(a) $\rho \ge 0$ *and* $\int_\Omega \rho dx = 1$;
(b) *for some fixed* $M_2 > 0$, $|\int_\Omega b_n \rho dx| \le M_2$ *for* $n = 1, \dots, \infty$.

Proof. Since $u_* \ge 0$ and $\int_\Omega u_* dx > 0$, there must exist some $\delta > 0$ such that

$$\mathcal{V} = \{x \in \Omega | u_* > 2\delta\} \text{ has finite positive measure.}$$

On the other hand, by Egorov's theorem [12] on a.e. convergence, there must exist a subset $\mathcal{W} \subset \mathcal{V}$, such that
(a') $|\mathcal{V} - \mathcal{W}| \le |\mathcal{V}|/2$ and hence $|\mathcal{W}| > 0$;
(b') $u_n \to u_*$ uniformly on $\mathcal{W}$.
Then there exists some integer K, such that for any $n > K$, we have $u_n > \delta$ on $\mathcal{W}$. Define

$$\rho(x) = \frac{1_{\mathcal{W}}(x)}{|\mathcal{W}|} \in L^2(\Omega).$$

Then $\int_\Omega \rho dx = 1$, and for any $n > K$,

$$\int_\Omega b_n^2 \rho dx = \int_\Omega b_n^2 \frac{1_{\mathcal{W}}(x)}{|\mathcal{W}|} dx = \frac{1}{|\mathcal{W}|\delta^p} \int_{\Omega \cap \mathcal{W}} b_n^2 \delta^p dx \le \frac{1}{|\mathcal{W}|\delta^p} \int_\Omega b_n^2 u_n^p dx \le \frac{M_1}{|\mathcal{W}|\delta^p}.$$

By the Schwarz inequality in probability theory, $\mathcal{E}[X]^2 \le \mathcal{E}[X^2]$, where X is the stochastic variable and $\mathcal{E}$ represents expectation, we have

$$\left| \int_\Omega b_n \rho dx \right| \le \left(\int_\Omega b_n^2 \rho dx \right)^{\frac{1}{2}} \le \left(\frac{M_1}{|\mathcal{W}|\delta^p} \right)^{\frac{1}{2}}.$$

Define $M_2 = \max\{|\int_\Omega b_1 \rho dx|, \dots, |\int_\Omega b_K \rho dx|, (\frac{M_1}{|\mathcal{W}|\delta^p})^{\frac{1}{2}}\}$. Then we get the conclusion. ∎

Proof of Theorem 3.1. If $I = 0$ a.e. $x \in \Omega$, then by formula (3.9), $c_i = 0, i = 1, \dots, N$. Hence $b = 0; c_i = 0, i = 1, \dots, N; u_1 = 1, u_j = 0, j = 2 : N$ is a minimizer. Otherwise, we take $b = 0,\ u_1 = 1,\ u_j = 0,\ j = 2 : N, c_1 = \int_\Omega I dx/|\Omega|,\ c_j = 0,\ j = 2 : N$, then $E(U, b, c) = \lambda(N + (N-1)w) \int_\Omega I^2 dx + \lambda w \int_\Omega (I - c_1)^2 dx < \infty$. Then the infimum of the energy must be finite.

Let $(U^n, b^n, c^n) \subset \mathrm{adm}_N$ be a minimizing sequence for energy (3.8), that is, $E(U^n, b^n, c^n) \to \inf E(U, b, c)$ as $n \to \infty$. Then there exists a constant $M_3 > 0$, such that

$$E(U^n, b^n, c^n) = \sum_{i=1}^N \lambda \int_\Omega \left((I - b^n c_i^n)^2 + w(I - c_i^n)^2 \right) (u_i^n)^p dx + \mu \int_\Omega |\nabla b^n|^2 dx + \sum_{i=1}^N \int_\Omega |\nabla u_i^n| dx \le M_3.$$

Then, each term of $E(U^n, b^n, c^n)$ is bounded, i.e.,

$$\lambda \int_\Omega (I - b^n c_i^n)^2 (u_i^n)^p dx \le M_3, \tag{3.10}$$

$$\mu \int_\Omega |\nabla b^n|^2 dx \le M_3, \tag{3.11}$$

$$\int_\Omega |\nabla u_i^n| dx \le M_3. \tag{3.12}$$

Since u_i^n satisfies condition (3.6), we have $\|u_i^n\|_{L^1(\Omega)} = \int_\Omega u_i^n dx \le |\Omega|$. From (3.12), it follows that $\{u_i^n\}$ is uniformly bounded in $\mathrm{BV}(\Omega)$ for each $i = 1, \ldots, N$. By the compactness property of BV space, up to a subsequence also denoted by $\{u_i^n\}$ after relabeling, there exists a function $u_i^* \in \mathrm{BV}(\Omega)$ such that

$$\begin{aligned} &u_i^n \to u_i^* \ \text{ strongly in } L^1(\Omega);\\ &u_i^n \to u_i^* \ \text{ a.e. } x \in \Omega;\\ &\nabla u_i^n \rightharpoonup \nabla u_i^* \ \text{ in the sense of measure.} \end{aligned}$$

Then by the lower semicontinuity of total variation,

$$\int_\Omega |\nabla u_i^*| dx \le \liminf_{n\to\infty} \int_\Omega |\nabla u_i^n| dx. \tag{3.13}$$

Meanwhile since u_i^n satisfies constraints (3.6) and (3.7), by convergence result, u_i^* also satisfies (3.6) and (3.7).

According to formula (3.9), we can derive that

$$0 \le c_i^n = \|I\|_{L^\infty(\Omega)}.$$

By the boundedness of sequence $\{c_i^n\}$, we can obtain a subsequence, also denoted by $\{c_i^n\}$, and a constant c_i^* such that

$$c_i^n \to c_i^* \ \text{ uniformly.}$$

By formula (3.9), we have

$$\begin{cases} c_i^* = \dfrac{\displaystyle\int_\Omega I(u_i^*)^p dx}{\displaystyle\int_\Omega (u_i^*)^p dx}, & \text{if} \displaystyle\int_\Omega (u_i^*)^p dx > 0,\\ c_i^* = 0, & \text{otherwise.} \end{cases}$$

We claim that there exists some i such that c_i^* is a positive constant. Since $\int_\Omega I dx > 0$ and $I \ge 0$, there exists a subset $\mathcal{P} \subset \Omega$ with positive measure such that $I > \delta' > 0$ on $\mathcal{P}$. Meanwhile, since $0 \le u_i^* \le 1$, and $\sum_{i=1}^N u_i^* = 1$, there exists some i and a subset $\mathcal{P}_1 \subset \mathcal{P}$ such that $\int_{\mathcal{P}_1} (u_i^*)^p dx > \epsilon' > 0$. Then

$$c_i^* = \frac{\displaystyle\int_\Omega I(u_i^*)^p dx}{\displaystyle\int_\Omega (u_i^*)^p dx} \ge \frac{\displaystyle\int_{\mathcal{P}_1} I(u_i^*)^p dx}{|\Omega|} \ge \frac{\delta' \epsilon' |\mathcal{P}_1|}{|\Omega|}.$$

Since $\int_\Omega I^2 (u_i^n)^p dx \le \int_\Omega I^2 dx$, together with inequality (3.10), and using the inequality $(a_1 - a_2)^2 \le 2(a_1^2 + a_2^2)$, we get

$$\int_\Omega (b^n c_i^n)^2 (u_i^n)^p dx = (c_i^n)^2 \int_\Omega (b^n)^2 (u_i^n)^p dx \le M_4.$$

We note that for some i, c_i^* is positive constant, and then there must be a subsequence $\{c_i^n\}$ which has positive lower bound. Hence we get

$$\int_\Omega (b^n)^2 (u_i^n)^p dx \le M_5.$$

Then by Lemma 3.2 there exists some $\rho(x) \geq 0$ with $\int_\Omega \rho dx = 1$, some constant $M_6 > 0$ such that

$$\left| \int_\Omega b^n \rho dx \right| \leq M_6.$$

Then by the generalized Poincaré inequality [11] on Ω,

$$\|b^n - \langle b^n, \rho \rangle\|_{L^2(\Omega)} \leq M_7 \|\nabla b^n\|_{L^2(\Omega)}.$$

Together with inequality (3.11), one concludes that

$$\|b^n\|_{H^1(\Omega)} = \|b^n\|_{L^2(\Omega)} + \|\nabla b^n\|_{L^2(\Omega)} \leq M_8.$$

By the L^2-weak compactness of bounded H^1-sequence, there is a subsequence still denoted by $\{b^n\}$ after relabeling, and a function $b^* \in H^1(\Omega)$ such that

$$\begin{aligned} &b^n \to b^* \ \text{ strongly in } L^2(\Omega); \\ &b^n \to b^* \ \text{ a.e. } x \in \Omega; \\ &b^n \rightharpoonup b^* \ \text{ weakly in } H^1(\Omega). \end{aligned}$$

Then by the lower semicontinuity,

$$\int_\Omega |\nabla b^*|^2 dx \leq \liminf_{n\to\infty} |\nabla b^n|^2 dx. \tag{3.14}$$

Finally, since $u_i^n \to u_i^*$, $b^n \to b^*$ a.e. x in Ω, and $c_i^n \to c_i^*$, Fatou Lemma gives

$$\int_\Omega \left((I - b^* c_i^*)^2 + w(I - c_i^*)^2\right)(u_i^*)^p dx \leq \liminf_{n\to\infty} \int_\Omega \left((I - b^n c_i^n)^2 + w(I - c_i^n)^2\right)(u_i^n)^p dx.$$

(3.15)

Combining inequalities (3.13), (3.14), and (3.15) for all i, on a suitable subsequence, we have established that

$$E(U^*, b^*, c^*) \leq \liminf_{n\to\infty} E(U^n, b^n, c^n) = \inf E(U, b, c), \tag{3.16}$$

and hence (U^*, b^*, c^*) must be a minimizer. This completes the proof. ∎

Next we show the symmetry of the minimizer of E. We consider S_N to denote the permutation group of $\{1, \ldots, N\}$. Each permutation $\gamma \in S_N$ is defined as a one to one map $\gamma : \{1, \ldots, N\} \to \{1, \ldots, N\}$ such that $\{\gamma(1), \ldots, \gamma(N)\}$ is a rearrangement of $\{1, \ldots, N\}$. Denote $U_\gamma = (u_{\gamma(1)}, \ldots, u_{\gamma(N)})$, $c_\gamma = (c_{\gamma(1)}, \ldots, c_{\gamma(N)})$. We have the following theorem.

THEOREM 3.3. *For any permutation $\gamma \in S_N$, $E(U_\gamma, b, c_\gamma) = E(U, b, c)$. In particular, suppose that*

$$(U^*, b^*, c^*) = \text{argmin}_{(U,b,c)\in \text{adm}_N} E(U, b, c)$$

is a minimizer. Then for any $\gamma \in S_N$, $(U_\gamma^*, b^*, c_\gamma^*)$ is also a minimizer of E.

The proof of this theorem is straightforward, and hence it is omitted.

4. Energy minimization. In this section, we present a numerical algorithm to minimize the proposed energy E. We first introduce the simplified notation

$$d_i(x) = (I(x) - b(x)c_i)^2 + w(I(x) - c_i)^2$$

and simplify the energies as

$$E(U, b, c) = \sum_{i=1}^{N} \lambda \int_\Omega d_i u_i^p dx + \mu \int_\Omega |\nabla b|^2 dx + \sum_{i=1}^{N} \int_\Omega |\nabla u_i| dx. \tag{4.1}$$

We use an alternative minimization method to minimize energy E. In the minimization scheme, we fix c and U, and update b, and then we fix c and b, and update U. Since c is defined as in (3.9), it is calculated based on the current value of U. Now we only need to describe the minimization of the energy with respect to b and U.

4.1. Minimization with respect to *b*. Taking the Gateaux derivative of E with respect to b, we get the associated Euler–Lagrange equation about b is

$$-\sum_{i=1}^{N} \lambda(I - bc_i)c_i u_i^p - \mu \Delta b = 0.$$

Let $J_1 = \sum_{i=1}^{N} c_i u_i^p$ and $J_2 = \sum_{i=1}^{N} c_i^2 u_i^p$. A fast approximated solution is provided by a Gauss–Seidel iterative scheme with the updating formula

$$b_{p,q} = \frac{\mu\left(b_{p+1,q} + b_{p-1,q} + b_{p,q+1} + b_{p,q-1}\right) + \lambda I_{p,q}(J_1)_{p,q}}{4\mu + \lambda(J_2)_{p,q}},$$

where p, q denotes the grid. For simplicity, we write it as

$$b = \frac{\mu\left(b^{so} + b^{no} + b^{ea} + b^{we}\right) + \lambda I J_1}{4\mu + \lambda J_2}, \tag{4.2}$$

where b^{so}, b^{no}, b^{ea}, and b^{we} means shift the matrix b one pixel in the south, north, east, and west directions, respectively.

4.2. Minimization with respect to *U*. To minimize energy E, it is difficult to solve U for general p. Here we consider only the case $p = 2$. We need to consider the optimization problem

$$\min_U E_1(U) = \frac{\lambda}{2} \sum_{i=1}^{N} \int_\Omega d_i u_i^2 dx + \sum_{i=1}^{N} \int_\Omega |\nabla u_i| dx, \tag{4.3}$$

subject to constraints (3.6) and (3.7). Note that we use a scaling of λ with a factor $\frac{1}{2}$ for simplicity. In the following we propose a novel numerical scheme by introducing the operator splitting method [20] to solve membership function U.

Since the objective function $E_1(U)$ is strictly convex and the feasible region is convex, there exists a unique global minimizer of (4.3). However, it is hard for us to write down the exact solution. In order to give an approximate numerical solution, first we do not consider the inequality constraints (3.6). By adding pointwise Lagrange multipliers $\alpha(x)$ (which is a function) to handle the equality constraints (3.7), the problem becomes

$$\min_{U,\alpha} E_2(U, \alpha) = \frac{\lambda}{2} \sum_{i=1}^{N} \int_\Omega d_i u_i^2 dx + \sum_{i=1}^{N} \int_\Omega |\nabla u_i| dx + \int_\Omega \alpha(x) \left(\sum_{i=1}^{N} u_i - 1 \right) dx. \tag{4.4}$$

Let $L = \nabla$ and $L^* = \nabla^T$ be the adjoint operator of ∇, and f is a function defined as $f(L(u_i)) = \int_\Omega |\nabla u_i| dx = \int_\Omega \sqrt{|\nabla_x u_i|^2 + |\nabla_y u_i|^2} dx$. Using these notations, the first order optimal conditions of problem (4.4) are

$$\mathbf{0} \in \lambda d_i u_i + \partial(f \circ L)(u_i) + \alpha, \tag{4.5}$$

$$0 = \sum_{i=1}^{N} u_i - 1. \tag{4.6}$$

By property of subdifference, $\partial(f \circ L)(u_i) = L^* \partial f(Lu_i)$. Let $L^* \mathbf{y}_i = L^* \partial f(Lu_i)$, and then $\mathbf{y}_i \in \partial f(Lu_i)$ which is equivalent to $Lu_i \in \partial f^*(\mathbf{y}_i)$ or $0 \in \partial f^*(\mathbf{y}_i) - Lu_i$. Hence u_i satisfies (4.5) if and only if there exists auxiliary variables $\mathbf{y}_i$ (vector-valued functions), such that

$$\mathbf{0} \in \partial f^*(\mathbf{y}_i) - Lu_i, \tag{4.7}$$

$$0 = \lambda d_i u_i + L^* \mathbf{y}_i + \alpha. \tag{4.8}$$

Although it is not easy to directly solve (4.7) and (4.8), we can apply the operator splitting method with two scalars $\tau, \theta > 0$, obtaining that (4.7) is equivalent to

$$\mathbf{0} \in \tau \partial f^*(\mathbf{y}_i) + \mathbf{y}_i - \mathbf{t}_i, \tag{4.9}$$

$$\mathbf{t}_i = \mathbf{y}_i + \tau L u_i, \tag{4.10}$$

and (4.8) is equivalent to

$$0 = \theta L^* \mathbf{y}_i + v_i - u_i, \tag{4.11}$$

$$u_i = v_i - \theta(\lambda d_i u_i + \alpha), \tag{4.12}$$

where $\mathbf{t}_i$ and v_i are auxiliary variables.

Using the property of subdifference, (4.9) is also equivalent to

$$\mathbf{0} \in \tau \mathbf{y}_i + \partial f(\mathbf{y}_i - \mathbf{t}_i),$$

which is the optimality condition of

$$\min_{\mathbf{y}_i} \frac{\tau}{2} \|\mathbf{y}_i\|_2^2 + f(\mathbf{y}_i - \mathbf{t}_i). \tag{4.13}$$

It is easy to derive that problem (4.13) has the closed-form solution

$$\mathbf{y}_i = \min\left\{ \|\mathbf{t}_i\|_2, \frac{1}{\tau} \right\} \frac{\mathbf{t}_i}{\|\mathbf{t}_i\|_2}. \tag{4.14}$$

The similar formula as (4.14) is also derived in [21, 30] by operator splitting.

From (4.11) and (4.12) we get the formulas for membership function u_i and auxiliary variable v_i

$$v_i = u_i - \theta L^* \mathbf{y}_i, \tag{4.15}$$

$$u_i = \frac{v_i - \theta\alpha}{1 + \lambda\theta d_i}. \tag{4.16}$$

We can solve the Lagrange multipliers α. Since u_i satisfies Euler–Lagrange equation (4.6), we have

$$\sum_{i=1}^{N} \frac{v_i - \theta\alpha}{1 + \lambda\theta d_i} = 1,$$

then

$$\alpha = \frac{\sum_{i=1}^{N} \frac{v_i}{1+\lambda\theta d_i} - 1}{\theta \sum_{i=1}^{N} \frac{1}{1+\lambda\theta d_i}}. \tag{4.17}$$

Substituting α into the formula of u_i gives

$$u_i = \frac{v_i}{1 + \lambda\theta d_i} - \frac{\sum_{j=1}^{N} \frac{v_j}{1+\lambda\theta d_j} - 1}{\sum_{j=1}^{N} \frac{1+\lambda\theta d_i}{1+\lambda\theta d_j}}.$$

Then second we can apply the inequality constraints (3.6) by projecting u_i on [0,1],

$$\hat{u}_i := \min\{\max\{u_i, 0\}, 1\}. \tag{4.18}$$

Finally $\hat{u}_i$ gives an approximate numerical solution for the membership function.

Sum up (4.10), (4.14), (4.15), and (4.18), the minimization problem with respect to U can be solved by the following alternative iterations:

$$\mathbf{y}_i = \min\left\{\frac{1}{\tau}, \|\mathbf{y}_i + \tau\nabla u_i\|_2\right\} \frac{\mathbf{y}_i + \tau\nabla u_i}{\|\mathbf{y}_i + \tau\nabla u_i\|_2}, \tag{4.19}$$

$$v_i = u_i - \theta\nabla^T \mathbf{y}_i, \tag{4.20}$$

$$u_i = \min\left\{\max\left\{\frac{v_i}{1 + \lambda\theta d_i} - \frac{\sum_{j=1}^{N} \frac{v_j}{1+\lambda\theta d_j} - 1}{\sum_{j=1}^{N} \frac{1+\lambda\theta d_i}{1+\lambda\theta d_j}}, 0\right\}, 1\right\}. \tag{4.21}$$

4.3. Implementation. The algorithm of minimizing E can be summarized in the following six steps:

- Step 1: Initialize the membership functions u_i by random matrices following a uniform distribution at $[0, 1]$ and then normalize them such that the constraints (3.6) and (3.7) are both satisfied. Initialize b as a matrix with all entries equal to 1. Set $v_i = u_i, \mathbf{y}_i = \mathbf{0}$ for each i and $p = 2$.
- Step 2: Update c_i by formula (3.9).
- Step 3: Update the function b by Gauss–Seidel iteration (4.2).
- Step 4: Update the auxiliary variables $\mathbf{y}_i$ by formula (4.19).
- Step 5: Update the auxiliary variables v_i by formula (4.20).
- Step 6: Update the membership functions u_i by formula (4.21).

  Repeat Steps 2–6 until termination. The termination criterion is as follows:

$$\|c_{new} - c_{old}\| \le \epsilon$$

  where $c = (c_1, \ldots, c_N)$ is the vector of centers, $\|\cdot\|$ denotes the Euclidean distance, and ϵ is a small positive number defined by the user.

Remark that, generally Steps 2–6 are executed once one by one. But if more regularity (smoothness) on bias field b is required, we can iterate b several times in each loop.

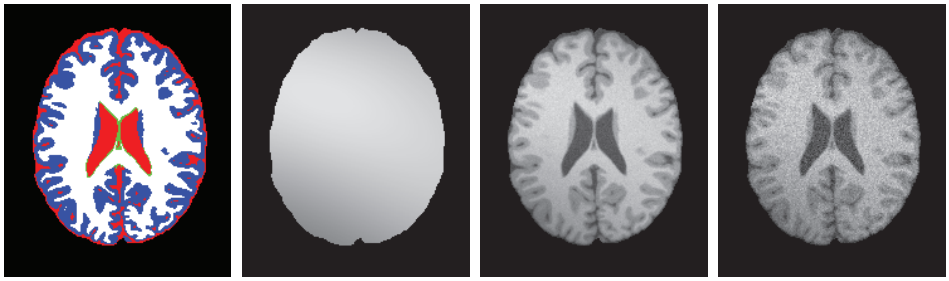

(a) (b) (c) (d)

FIG. 5.1. *Simulated MR images.* (a) *Ground truth of segmentation;* (b) *ground truth of bias field b;* (c) *MR image with* 3% *noise and INU* 100%*;* (d) *MR image with* 9% *noise and INU* 100%.

5. Experimental results. We test our algorithms on medical images and natural images. In all the experiments, we set the termination criterion $\epsilon = 10^{-4}$ and fix $\tau = 1$, $\theta = 0.1$; the other parameters should be tuned in each case. For MR images, since the bias field is very smooth actually, we iterate b for five times in each loop. While for all the other images, we iterate b one time in each loop which seems to be enough to get satisfactory results. The segmentation results of the proposed algorithm and the fuzzy c-means algorithm [4] are obtained by checking the maximum value of their membership functions. Note that the bias corrected image is computed by formula I/b.

5.1. Synthetic MR images. We test our algorithms on a simulated brain MR image obtained from the McGill Brain Web site (http://www.bic.mni.mcgill.ca/brainweb/). The MR image and the ground-truth segmentation are shown in Figure 5.1. In the segmentation ground truth figure, we see that the image indeed contains five classes: background (black), white matter (white), gray matter (blue), cerebrospinal fluid (red), and glial matter (green). Since the glial matter is relatively small, we consider classifying the three main tissues: white matter (WM), gray matter (GM), and cerebrospinal fluid (CSF). Here we add the noise with levels 3% and 9%, and intensity nonuniformity (INU) 100% (i.e., the multiplied bias field is scaled to a range between 0.5 and 1.5). The tested bias field is given in Figure 5.1(b). The noisy images are shown in Figures 5.1(c) and 5.1(d), respectively.

Figure 5.2 shows the segmentation results and the bias fields estimation using the proposed algorithm on the two synthetic noisy MR images in Figures 5.1(c) and 5.1(d). From these figures, it can be seen that the proposed algorithm performs quite well even when the noise level is high.

For comparison, we use the segmentation accuracy (SA) and root mean square (RMS) error to evaluate the accuracy of the algorithms. The SA and RMS are defined as follows:

$$\text{SA} = \frac{\text{Number of correctly classified pixels}}{\text{Total number of pixels}} \times 100\%,$$

$$\text{RMS} = \sqrt{\frac{\|b - b_r\|_2^2}{\text{Area of } \Omega}},$$

where b_r is the ground truth and b is the estimated bias field. In the experiments, we run each method ten times using different initial guesses. The average results are reported in Table 5.1. The method proposed by Li et al. [17] is used for comparison.

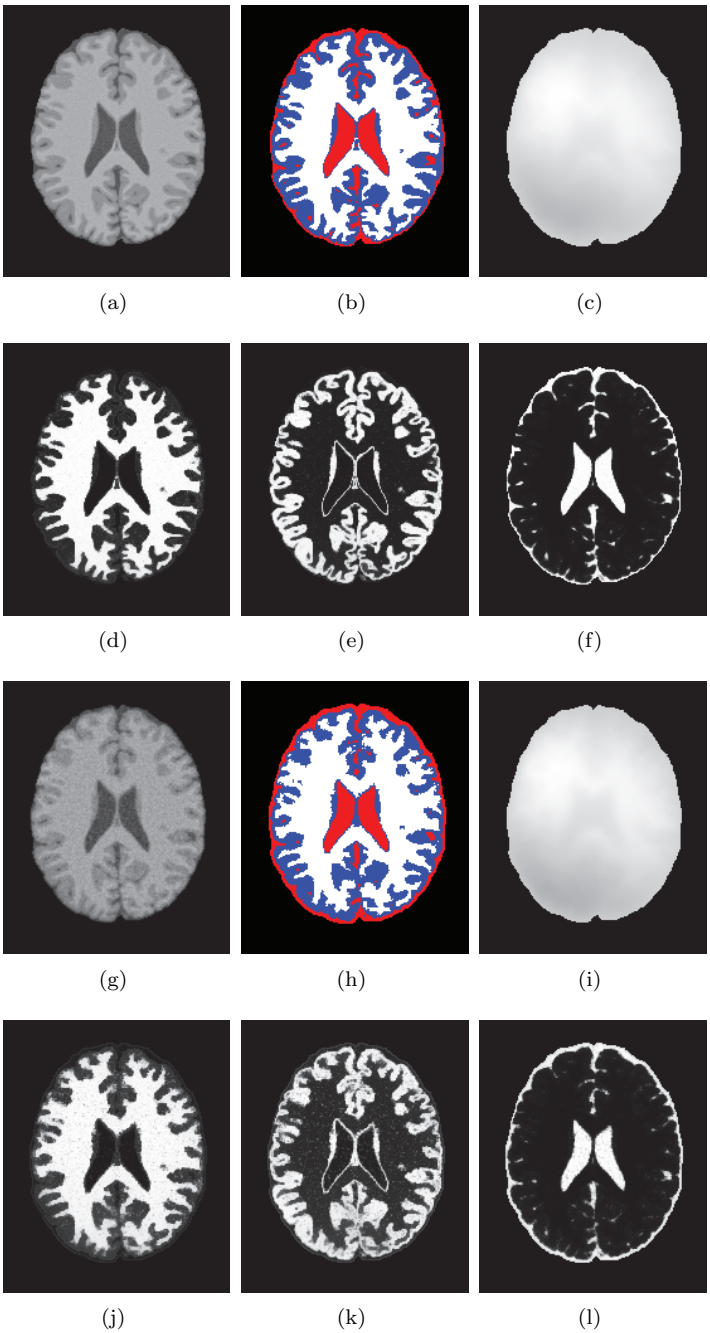

FIG. 5.2. *Results of the proposed algorithm for simulated MR images with* 3% *and* 9% *noise. The first row is the results for* 3% *noise and the second row is for* 9% *noise:* (a) *and* (g) *the estimated bias fields;* (b) *and* (h) *the bias corrected images;* (c) *and* (i) *the segmentation results;* (d) *and* (j) *the membership functions of WM;* (e) *and* (k) *the membership functions of GM;* (f) *and* (l) *the membership functions of CSF. Parameters for* 3% *noise image are* $\lambda = 0.02, w = 0.001, \mu = 1000$, *and for* 9% *noise image is* $\lambda = 0.01, w = 0.001, \mu = 2000$.

TABLE 5.1
Comparison of the proposed algorithm and the level method proposed by Li et al. in [17] *for Figures* 5.1(c) *and* 5.1(d).

	3% noise		9% noise	
	Proposed method	Method in [17]	Proposed method	Method in [17]
SA	96.50%	93.12%	91.46%	86.57%
RMS	0.0335	0.0404	0.0412	0.0520

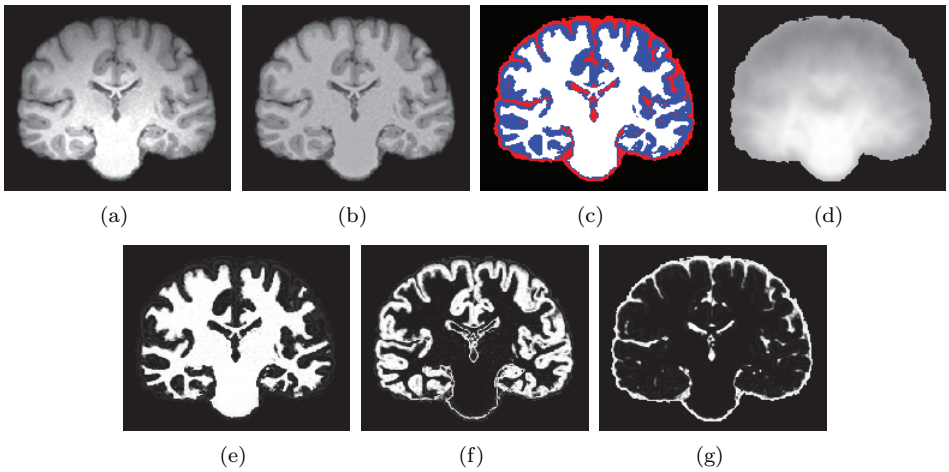

FIG. 5.3. *Results of Algorithm* 1 *for real* 3*T MR image.* (a) *The real* 3*T MR image;* (b) *the estimated bias field;* (c) *bias corrected image;* (d) *segmentation;* (e) *the membership function of WM;* (f) *the membership function of GM;* (g) *the membership function of CSF. Parameters:* $\lambda = 0.2, w = 0.001, \mu = 1000$.

We see from Table 5.1 that the proposed algorithm has quite high SA values. We remark that the method of Li et al. was presented in a level set formulation in [17], which does not allow random initialization of the level set function. It is somewhat sensitive to initialization; therefore, the average SA of their method is lower than that of our method. Meanwhile, the RMS of their method is higher than that of our method.

5.2. Real MR images. Next we apply our method to a real 3T MR image in Figure 5.3(a). It is clear that the intensity inhomogeneity appears in this figure. The computed bias field is shown in Figure 5.3(b). The corresponding corrected image is displayed in Figure 5.3(c). The segmentation result is shown in Figure 5.3(d). Figures 5.3(e), 5.3(f), and 5.3(g) show the membership functions of WM, GM, and CSF, respectively. We see from Figures 5.3(d)–5.3(g) that the segmentation performance is quite consistent with brain anatomy by visual inspection.

5.3. Natural images. In this subsection, we test the performance of the proposed algorithm for natural images with intensity inhomogeneity. The three test images in the first column of Figure 5.4 are from Matlab. In these figures, the "peppers" image is contaminated by a Gaussian zero mean noise with the standard deviation 10; the "rice" image and the "coins" image are contaminated by Gaussian zero mean noise with the standard deviation 20. Obvious intensity inhomogeneities can be seen from the images in Figures 5.4(a), 5.4(e), and 5.4(i). The segmentation results by the proposed algorithm are shown in the second column of Figure 5.4. We find that the

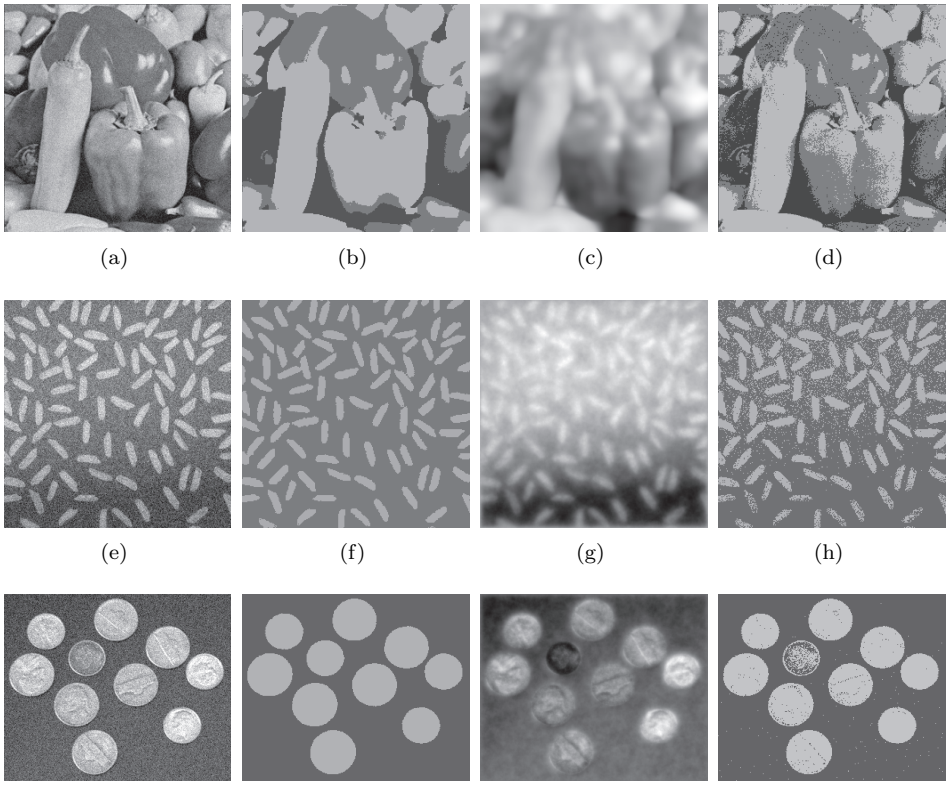

FIG. 5.4. *The first column: test images; the second column: the segmentation by the proposed algorithm; the third column: the functions b in the proposed algorithm; the fourth column: the segmentation by the FCM algorithm. Parameters for peppers image:* $\lambda = 0.0008, w = 0.01, \mu = 1000$*; rice image:* $\lambda = 0.0015, w = 0.001, \mu = 100$*; coins image:* $\lambda = 0.001, w = 0.01, \mu = 100$.

segmentation performance of the proposed algorithm is desirable. The third column of Figure 5.4 displays the functions b of the three tested images. It can be seen that the computed function b is smooth. The results of the FCM algorithm are not as accurate as the proposed method due to the presence of intensity inhomogeneity. Moreover, the FCM algorithm is quite sensitive to noise, as can be seen from the segmentation results in the last column.

In Figure 5.5, we test the performance of the proposed algorithm for more natural images. In these images, they are seriously affected by intensity inhomogeneity. We see from the second column of Figure 5.5 that the performance of the proposed algorithm is still quite well. In contrast, the performance of the FCM algorithm is quite poor (see the last column of Figure 5.5), which shows that the FCM algorithm is sensitive to intensity inhomogeneity.

5.4. Color images. The proposed method can easily be extended to color image segmentation in the presence of intensity inhomogeneity. We consider a color image I as a vector valued function: $I : \Omega \to \mathbb{R}^3$. The image model in (3.1) can be extended to color images as below:

$$I_j(x) = b(x)c_{i,j} + n_j(x), \quad j = 1, 2, 3, \quad x \in \Omega_i,$$

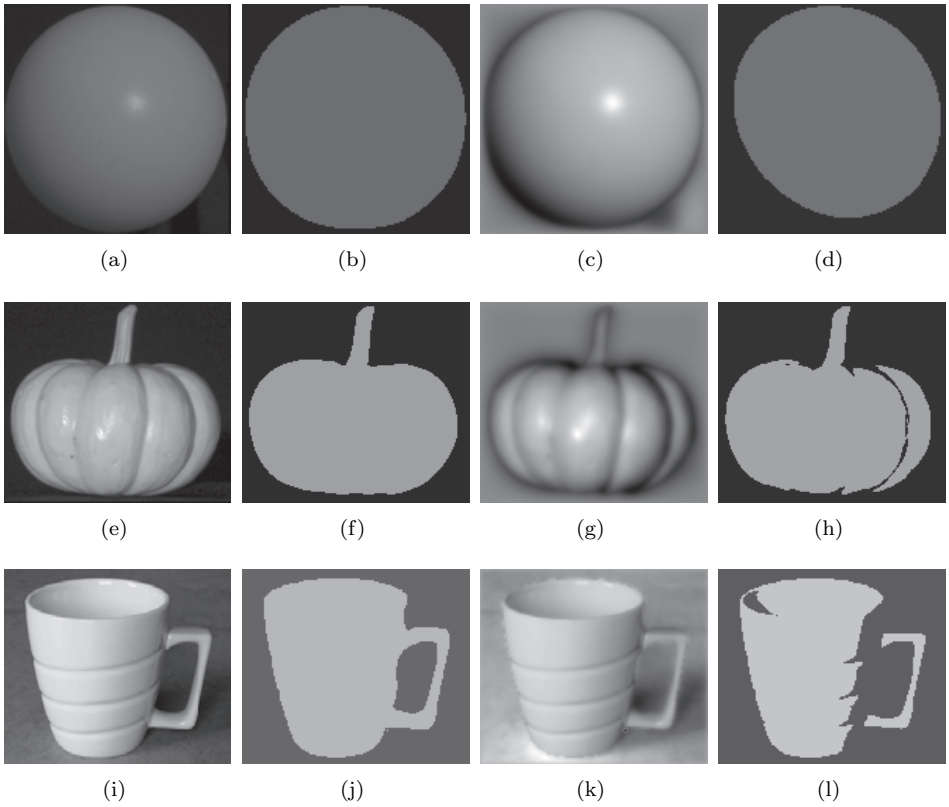

FIG. 5.5. *The first column: test images; the second column: the segmentation by the proposed algorithm; the third column: the functions b in the proposed algorithm; the fourth column: the segmentation by the FCM algorithm. Parameters for orange image:* $\lambda = 0.1, w = 0.001, \mu = 1000$*; pumpkin image:* $\lambda = 0.01, w = 0.001, \mu = 1000$*; cup image:* $\lambda = 0.01, w = 0.001, \mu = 100$.

where $\{\Omega_i\}_{i=1}^N$ is a partition of the image domain Ω, b is a smooth function, and $c_i = (c_{i,1}, c_{i,2}, c_{i,3})$ is a constant vector that denotes color intensity in the red, green, and blue channels. Similar to the case of gray images, the constants $c_{i,j}$ are given by

$$c_{i,j} = \frac{\int_\Omega I_j(x) u_i^p(x) dx}{\int_\Omega u_i^p(x) dx}. \tag{5.1}$$

We define the distance $d_{ij}(x)$ as

$$d_{ij}(x) = (I_j(x) - b(x)\ c_{ij})^2 + w(I_j(x) - c_{ij})^2$$

for each channel j. Then d_i is defined as the average of d_{ij} in the three channels, i.e.,

$$d_i = \frac{d_{i1} + d_{i2} + d_{i3}}{3}.$$

Then the Gauss–Seidel iteration scheme of b is given by

$$b = \frac{\mu\,(b^{so} + b^{no} + b^{ea} + b^{we}) + \lambda I J_1}{4\mu + \lambda J_2}, \tag{5.2}$$

where $b^{so}, b^{no}, b^{ea}, b^{we}$ are as in (4.2) and

$$J_1 = \sum_{j=1}^{3}\sum_{i=1}^{N} c_{ij} u_i^p, J_2 = \sum_{j=1}^{3}\sum_{i=1}^{N} c_{ij}^2 u_i^p.$$

Thus, the numerical algorithm for a color image can be derived similar to the case of a gray scale image using the new formulas for b, c, and d.

In Figure 5.6, we show the performance of the proposed algorithm for color images. For comparison, we also show the segmentation results by the FCM algorithm.

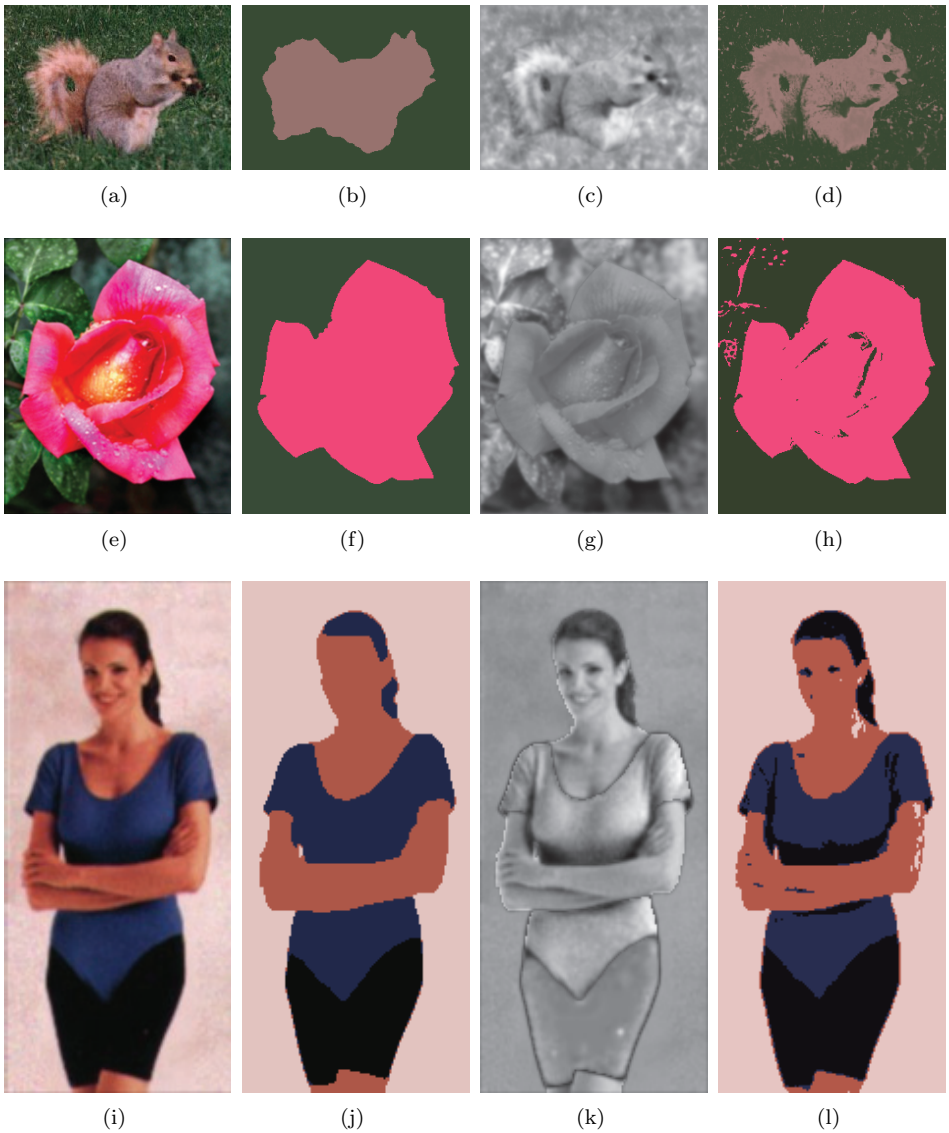

FIG. 5.6. *The first column: test images; the second column: the segmentation by the proposed algorithm; the third column: the functions b in the proposed algorithm; the fourth column: the segmentation by the FCM algorithm. Parameters for squirrel image:* $\lambda = 0.0005, w = 0.001, \mu = 100$*; rose image:* $\lambda = 0.0005, w = 1, \mu = 10$*; woman image:* $\lambda = 0.01, w = 0.1, \mu = 10$.

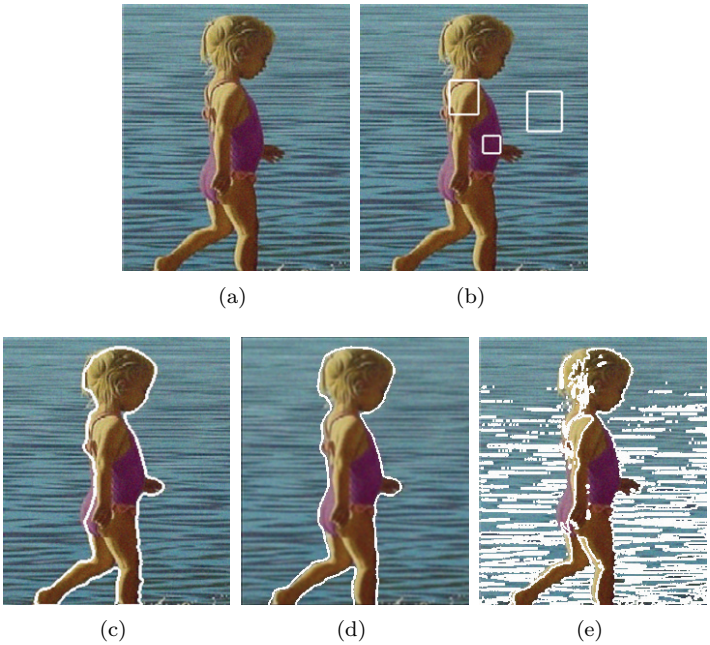

FIG. 5.7. (a) *The original image;* (b) *prior information (the two rectangles on the body are foreground and the rectangle on the ocean is background);* (c) *segmentation by the soft Mumford–Shah model* [31]; (d) *segmentation by the proposed algorithm;* (e) *segmentation by the FCM algorithm. Parameters for sea girl image:* $\lambda = 0.003, w = 0.001, \mu = 10$.

From the results shown in the second column of Figure 5.6, it can clearly be seen that the proposed method achieves desirable segmentation results in the presence of intensity inhomogeneity. In contrast, the FCM algorithm is seriously misled by intensity inhomogeneity; see the last column of Figure 5.6.

In the next experiment, we compare the proposed algorithm with the soft Mumford–Shah model in [31]. A natural color image tested in [31] is shown in Figure 5.7(a). The prior information on the foreground and the background is used in the soft Mumford–Shah model [31]; see Figure 5.7(b). The segmentation results by the soft Mumford–Shah model, the proposed algorithm, and the FCM algorithm are displayed in Figures 5.7(c), 5.7(d), and 5.7(e), respectively. Without the prior information, the proposed algorithm gives a better segmentation result than the soft Mumford–Shah model. The segmentation given by the FCM algorithm is quite poor.

In our algorithm, five manual parameters are needed. The two parameters τ and θ come from the use of the operator splitting method which is not crucial in speeding up the convergence. We set $\tau = 1$ and $\theta = 0.1$ in all the experiments. In fact, a small change of these two parameters works quite well. The other three parameters λ, w, μ should be tuned in each experiment since they are the weight of the terms in the energy (3.8). There are some rules. For a noisy image, more regularization of U is needed to smooth the noise, so one should decrease λ (the coefficient of fidelity term) since the coefficient of the regularization term of U in (3.8) is fixed as 1. w and μ are related with the smoothness of the bias field. For an image with serious bias field, it is better to decrease w and increase μ.

We compared our method with using Chambolle's dual method [8] and the Split Bregman method [13] to solve U in the whole algorithm, and we find that our method

converges as fast as Chambolle's dual method but a little faster than the Split Bregman method. The main reason is that the use of the Split Bregman method needs to update more auxiliary variables when solving U.

6. Conclusion. In this paper, based on the assumption that a piecewise smooth image can be approximated by the product of a piecewise constant function and a smooth function, we develop the Mumford–Shah model in fuzzy segmentation framework. We show the existence and symmetry of minimizers for the proposed energy minimization problem. An iterative algorithm is developed to solve such an energy minimization problem efficiently. Experimental results demonstrate the ability of the proposed method to segment images with intensity inhomogeneities. The study of the convergence of the proposed algorithm will be our future work.

REFERENCES

[1] M. N. Ahmed, S. M. Yamany, N. Mohamed, A. A. Farag, and T. Moriarty, *A modified fuzzy C-means algorithm for bias field estimation and segmentation of MRI data*, IEEE Trans. Med. Imag., 21 (2002), pp. 193–199.

[2] G. Aubert and P. Kornprobst, *Mathematical Problems in Image Processing: Partial Differential Equations and the Calculus of Variations (Applied Mathematical Sciences)*, 2nd ed., Springer-Verlag, Berlin, 2006.

[3] J. C. Bezdek, *A convergence theorem for the fuzzy ISODATA clustering algorithms*, IEEE Trans. Pattern Anal. Machine Intell., 2 (1980), pp. 1–8.

[4] J. C. Bezdek, L. O. Hall, and L. P. Clarke, *Review of MR image segmentation techniques using pattern recognition*, Med. Phys., 20 (1993), pp. 1033–1048.

[5] X. Bresson, S. Esedoglu, P. Vandergheynst, J.-P. Thiran, and S. Osher, *Fast global minimization of the active contour/snake model*, J. Math. Imaging Vision, 28 (2007), pp. 151–167.

[6] X. Bresson and T. F. Chan, *Non-local unsupervised variational image segmentation models*, UCLA CAAM Report 08-67.

[7] V. Caselles, R. Kimmel, and G. Sapiro, *Geodesic active contours*, Internat. J. Comput. Vision, 1 (1997), pp. 61–79.

[8] A. Chambolle, *An algorithm for total variation minimization and applications*, J. Math. Imaging Vision, 20 (2004), pp. 89–97.

[9] T. F. Chan and L. A. Vese, *Active contour without edges*, IEEE Trans. Image Process., 10 (2001), pp. 266–277.

[10] G. Dogan, P. Morin, and R. H. Nochetto, *A variational shape optimization approach for image segmentation with a Mumford–Shah functional*, SIAM J. Sci. Comput., 30 (2008), pp. 3028–3049.

[11] L. C. Evans and R. F. Gariepy, *Measure theory and fine properties of functions*, Studies in Advanced Mathematics. CRC Press, Roca Baton, FL, 1992.

[12] G. B. Folland, *Real Analysis—Modern Techniques and Their Applications*, 2nd ed., John Wiley & Sons, New York, 1999.

[13] T. Goldstein and S. Osher, *The Split Bregman Method for L1 Regularized Problems*, UCLA CAAM Report 08-29.

[14] L. He and S. Osher, *Solving the Chan-Vese model by a multiphase level set algorithm based on the topological derivative*, Conf. on Scale Space and Variational Methods in Computer Vision, 2008, Lecture Notes in Comput. Sci., 4485 (2010), pp. 777–778.

[15] M. Hintermüller and A. Laurain, *Multiphase image segmentation and modulation recovery based on shape and topological sensitivity*, J. Math. Imaging Vision, 35 (2009), pp. 1–22.

[16] M. Hintermüller and W. Ring, *An inexact Newton-CG-type active contour approach for the minimization of the Mumford-Shah functional*, J. Math. Imaging Vision, 20 (2004), pp. 19–42.

[17] C. Li, R. Huang, Z. Ding, C. Gatenby, and D. Metaxas, *A variational level set approach to segmentation and bias correction of images with intensity inhomogeneity*, MICCAI 2008, Part II, LNCS 5242 (2008), pp. 1083–1091.

[18] C. Li, C.-Y. Kao, J.C. Gore, and Z. Ding, *Implicit active contours driven by local binary fitting energy*, in Proceedings of the IEEE Conference on Computer Vision and Pattern Recognition, IEEE Computer Society, Washington, DC, 2007, pp. 1–7.

[19] X. Li, L. Li, H. Lu, and Z. Liang, *Partial volume segmentation of brain magnetic resonance images based on maximum a posteriori probability*, Med. Phys., 32 (2005), pp. 2337–2345.
[20] P. L. Lions and B. Mercier, *Splitting algorithms for the sum of two nonlinear operators*, SIAM J. Numer. Anal., 16 (1979), pp. 964–979.
[21] S. Ma, W. Yin, Y. Zhang, and A. Chakraborty, *An efficient algorithm for compressed MR imaging using total variation and wavelets*, in Proceedings of the IEEE Conference on Computer Vision and Pattern Recognition, IEEE Computer Society, Alaska, 2008, pp. 1–8.
[22] B. Mory and R. Ardon, *Fuzzy region competition: A convex two-phase segmentation framework*, F. Sgallari, A. Murli, and N. Paragios, eds., SSVM 2007, Lecture Notes in Comput. Sci. 4485, 2007, pp. 214–226.
[23] B. Mory and R. Ardon, *Variational segmentation using fuzzy region competition and local non-parametric probability desity functions*, Computer Vision, 2007, ICCV 2007, IEEE 11th International Conference on Computer Vision, pp. 1–8.
[24] D. Mumford and J. Shah, *Optimal approximations by piecewise smooth functions and associated variational problems*, Comm. Pure Appl. Math., 42 (1989), pp. 577–685.
[25] K. Ni, X. Bresson, T.F. Chan, and S. Esedoglu, *Local Histogram Based Segmentation Using the Wasserstein Distance*, UCLA CAAM Report 08-47.
[26] M. Nikolova, S. Esedoglu, and T. F. Chan, *Algorithms for finding global minimizers of image segmentation and denoising models*, SIAM J. Appl. Math., 66 (2006), pp. 1632–1648.
[27] S. Osher and N. Paragios, *Geometric Level Set Methods in Imaging Vision and Graphics*, Springer-Verlag, Berlin, 2003.
[28] N. Paragios and R. Deriche, *Geodesic active regions for supervised texture segmentation*, Proceedings of International Conference on Computer Vision, 1999, pp. 22–25.
[29] D. L. Pham and J. L. Prince, *An adaptive fuzzy C-means algorithm for the image segmentation in the presence of intensity inhomogeneities*, Pattern Recognit. Lett., 20 (1998), pp. 57–68.
[30] C. M. Shen, *Geometric variational principle based image processing method*, Ph.D. thesis of East China Normal University (in Chinese), 2009.
[31] J. Shen, *A stochastic-variational model for soft Mumford-Shah segmentation*, Internat. J. Biomed. Imag., V2006 (2006), pp. 1–14.
[32] A. Tsai, A. Yezzi, and A. S. Willsky, *Curve evolution implementation of the Mumford-Shah functional for image segmentation, denoising, interpolation, and magnification*, IEEE Trans. Image Process., 10 (2001), pp. 1169–1185.
[33] L. A. Vese and T. F. Chan, *A multiphase level set framework for image segmentation using the Mumford and Shah Model*, Int. J. Comput. Vision, 50 (2002), pp. 271–293.
[34] U. Vovk, F. Pernus, and B. Likar, *A review of methods for correction of intensity inhomogeneity in MRI*, IEEE Trans. Med. Imag., 26 (2007), pp. 405–421.
[35] W. Wells, E. Grimson, R. Kikinis, and F. Jolesz, *Adaptive segmentation of MRI data*, IEEE Trans. Med. Imag., 15 (1996), pp. 429–442.
[36] S. C. Zhu and A. Yuille, *Region competition: Unifying snakes, region growing, and bayes/mdl for multiband image segmentation*, IEEE Trans. Pattern Anal. Machine Intell., 18 (1996), pp. 884–900.